A Regional Model Simulation of the 1991 Severe Precipitation Event over the Yangtze–Huai River Valley. Part I: Precipitation and Circulation Statistics

WEI-CHYUNG WANG, WEI GONG, AND HELIN WEI

Atmospheric Sciences Research Center, University at Albany, State University of New York, Albany, New York

(Manuscript received 6 July 1998, in final form 12 February 1999)

ABSTRACT

The summer Mei-yu event over eastern China, which is strongly influenced by large-scale circulation, is an important aspect of East Asian climate; for example, the Mei-yu frequently brings heavy precipitation to the Yangtze–Huai River valley (YHRV). Both observations and a regional model were used to study the Mei-yu front and its relation to large-scale circulation during the summer of 1991 when severe floods occurred over YHRV. This study has two parts: the first part, presented here, analyzes the association between heavy Mei-yu precipitation and relevant large-scale circulation, while the second part, documented by W. Gong and W.-C. Wang, examines the model biases associated with the treatment of lateral boundary conditions (the objective analyses and coupling schemes) used as the driving fields for the regional model.

Observations indicate that the Mei-yu season in 1991 spans 18 May–14 July, making it the longest Mei-yu period during the last 40 yr. The heavy precipitation over YHRV is found to be intimately related to the western Pacific subtropical high, upper-tropospheric westerly jet at midlatitudes, and lower-tropospheric southwest wind and moisture flux. The regional model simulates reasonably well the regional mean surface air temperature and precipitation, in particular the precipitation evolution and its association with the large-scale circulation throughout the Mei-yu season. However, the model simulates smaller precipitation intensity, which is due partly to the colder and drier model atmosphere resulting from excessive low-level clouds and the simplified land surface process scheme used in the present study.

1. Introduction

East Asia is located in the southeast of the Eurasian continent. It is bordered in the east by the Pacific Ocean and in the southwest by the Tibetan Plateau, which penetrates into the middle troposphere. These unique geographic features produce distinct climate characteristics over East Asia. Observational analyses indicate that this region has the strongest heat sources/sinks in the Northern Hemisphere and that the Tibetan Plateau creates vigorous dynamic and thermal forcing (Ye 1988), causing substantial atmospheric responses that result in several unique climate features (Domros and Peng 1988).

a. Mei-yu system

The most important climate feature over East Asia is the summer monsoon. As indicated in Tao and Chen (1987), the East Asian summer monsoon consists of several components: the monsoon trough (or ITCZ) over the South China Sea and the western Pacific Ocean; the convection along the monsoon trough; the cross-equatorial flow to east of 100°E; the cold anticyclone in Australia; the western Pacific subtropical high (WPSH); the upper-tropospheric northeasterly flow; the Mei-yu (and Baiu in Japan) front zones; and the midlatitude disturbances, which are associated with both the upper-tropospheric westerly jet and the blocking highs at higher latitudes. These components not only have a close relationship among themselves, but also interact with regional-scale circulation resulting from the characteristics of underlying surfaces, for example, terrain and coastlines (Tao and Chen 1987; Chen et al. 1991; Ding 1994).

The dominant characteristics of the East Asian summer monsoon are the seasonal variation of large-scale circulation and its associated persistent and heavy precipitation. Typically, as a result of the seasonal evolution of atmospheric circulation, the monsoon rain belt arrives in the southern China coast in early May, abruptly jumps to the north several times, reaches northeast China in early August, and quickly retreats to the south in the fall. In mid-June, the monsoon precipitation begins over the Yangtze–Huai River Valley (YHRV; see Fig. 1), which is known as Mei-yu or Plum rain. The characteristics of Mei-yu (the date of onset, and its length and intensity) exhibit substantial seasonal and interannual variabilities, and result in frequent regional flood and drought (Tao and Chen 1987; Ding 1994).

Corresponding author address: Dr. Wei-Chyung Wang, Atmospheric Sciences Research Center, SUNY at Albany, 251 Fuller Rd., Albany, NY 12203.
E-mail: wang@climate.cestm.albany.edu

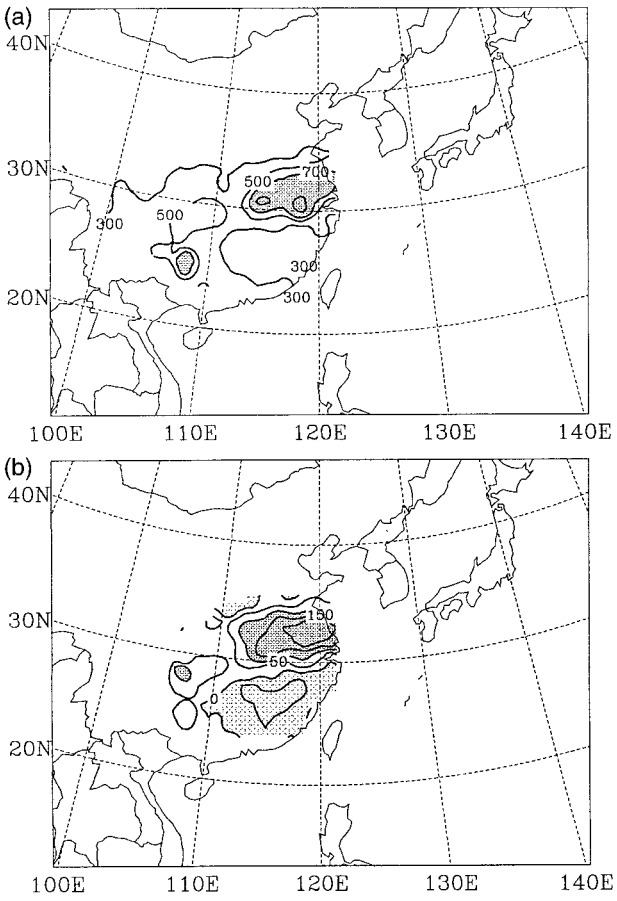

FIG. 1. (a) 1991 observed total precipitation (mm) during total Mei-yu season (18 May–13 Jul). Contours greater than 700 mm are densely shaded. (b) 1991 precipitation anomaly (percent) vs the 1981–90 climatological mean precipitation for the same period. Contours greater than 100% (less than 0%) are densely (lightly) shaded. The observations are based on the WMO surface station network archived at the National Center for Atmospheric Research. The geographical domain of the YHRV used in the present study is chosen to be within (30°–34°N; 105°–122°E).

The Mei-yu precipitation is the product of the Mei-yu front, which is quasi-stationary and is a characteristic of interaction between the (warm/moist) winds from the south and (cold/dry) airflow originating from the north (Lau and Li 1984). There are several characteristics of the large-scale circulation associated with the heavy Mei-yu precipitation. At 200 hPa, the ridge of South Asian high pressure, normally centered in the south of the Tibetan Plateau, extends to the east and coincides with the location of the Mei-yu front. Accompanying the South Asian high pressure is an anticyclonic circulation that consists of a westerly jet about 5°–8° north of the Yangtze River, and a northeasterly flow south of the Mei-yu front. This anticyclone provides a favorable divergence field to the underlying convective activity along the Mei-yu front. In the midtroposphere, the ridge of the WPSH, which usually determines the location where the warm air from the south meets the cold air from the north, stays stable at 20°–25°N with the Mei-yu front forming 5°–8° north of the ridge. In the lower troposphere around 850 hPa, a shearline occurs over YHRV. North of the shearline, cold anticyclonic air moves eastward frequently to the ocean, while in the south, warm and moist southwest monsoon flow, coming from the Indo-China peninsula, the South China Sea, and the western Pacific Ocean, reaches the Yangtze River valley along the shearline. In addition, frequently there is a strong low-level jet accompanying the heavy Mei-yu front (Chen and Yu 1988). This jet transports moist air into YHRV, and generates atmospheric instability, which is favorable for intensive convective activities (Chen 1982).

In an observational study, Yamazaki and Chen (1993) found that tropospheric circulation at all levels is closely related during the Baiu season in Japan. Specifically, they found that the southwesterly moisture flux, upper-tropospheric westerly jet, and low-level cyclonic shearline are closely related with the Baiu front. Therefore, we study the summer monsoon using the framework of the *Mei-yu system*, which includes: the Mei-yu front, the low-level southwest flow from the south, the WPSH, the upper-tropospheric westerly jet at midlatitude, and the stable blocking high(s) at higher latitudes.

b. Regional- and large-scale interaction

It is quite clear that the components of the Mei-yu system involve regional- and large-scale interaction. Understanding of the East Asian summer monsoon is much improved during the last few decades, due partly to the available observations (regular soundings and field campaigns, such as First Global Atmosphere Research Program Experiment/Monsoon Experiment) and GCM simulations (Sperber et al. 1994; Liang et al. 1995; Samel et al. 1995; Lau and Yang 1996; Liang and Wang 1998). However, an accurate prediction of monsoon precipitation is still a challenging task for the modeling community because of the complexities associated with the thermal and mechanical effects of mountain ranges and the land–sea contrast (Ding 1994). In addition, difficulties in simulating East Asian summer monsoon also arise from the multiscale interactions involving planetary scale (the WPSH and upper-tropospheric westerly jet), synoptic scale (Mei-yu front and its secondary circulation), and mesoscale (the ''southwest vortex'' originated in the east side of the Tibetan Plateau), and from the various physical and dynamical processes that govern the circulation characteristics of different scales at tropical, subtropical, and midlatitudes (Lau and Yang 1996; Wang 1997).

General circulation models have been shown to possess some ability to simulate large-scale climate features (Liang and Wang 1998). However, they are also known to have deficiencies in simulating regional circulation and precipitation over East Asia, due partly to their coarse resolution and inadequate physical parameteri-

zations. On the other hand, regional climate models, with finer resolution and more detailed physical parameterizations (especially those for mesoscale processes) can be used to evaluate multiscale interactions, and to improve the parameterizations for physical processes of regional importance.

Here we used the State University of New York at Albany (SUNYA) Regional Climate Model (RCM; Dudek et al. 1996), driven by lateral boundary forcing provided by objective analysis, to simulate the evolution of the Mei-yu system in 1991—a year in which severe floods occurred over YHRV. Our regional modeling effort is part of the U.S. Department of Energy sponsored regional model intercomparison project (Leung et al. 1999), which is intended to identify and understand the difference in model simulations with identical lateral boundary conditions. Parallel to providing input to the intercomparison project, we also conduct detailed diagnostics and additional sensitivity experiments to improve the regional models.

There were several regional model studies of the East Asian summer monsoon (Liu et al. 1996; Lau et al. 1998), but our study focuses on the evolution of the Mei-yu front and its association with the circulation components, as well as the consistency among the circulation components themselves. Specifically, we concentrate on the analysis of the association between anomalous precipitation and large-scale features of the WPSH, moisture flux, and low-level jets accompanying the Mei-yu front, and the upper-tropospheric westerly jet at midlatitudes, which are reported here. In a companion paper (Gong and Wang 2000), a series of sensitivity experiments were conducted to examine the model biases due to the treatment of lateral boundary and the physical parameterization related to cloud–radiation interaction. Section 2 describes the observed characteristics of the 1991 severe precipitation event over YHRV. A brief description of the regional model is given in section 3 while section 4 presents the simulation results. Note that in this paper we used the best choice of model configurations (the nesting procedure and the treatment of cloud–radiation scheme) as was concluded from the sensitivity experiments documented in Gong and Wang (2000). Highlights of the findings and discussion are summarized in section 5.

2. 1991 severe precipitation event over the Yangtze–Huai River valley

The 1991 precipitation event over YHRV has been extensively documented by Ding (1993). During the Mei-yu season, heavy rain occurred in this region and resulted in severe floods, perhaps one of the worst in this century with the amount being even greater than that in 1954. In addition, mesoscale activities were very active; for example, during 12–16 June, 13 cloud clusters and rainstorms were identified along the Mei-yu front.

TABLE 1. Onset and ending date of Mei-yu season (after Ding 1993).

Period	Onset date	Ending date
1991	2 Jun	14 Jul
1981–90	21 Jun	11 Jul
1951–90	18 Jun	9 Jul

Climatologically, the 1991 event is unique in at least three ways. First, the Mei-yu season over YHRV was long. As shown in Table 1, the onset started on 2 June and the ending date was 14 July, a period which is almost a factor of two longer than the climatological mean value of about 20 days for the previous few decades. There were only 2 yr on record in which a longer Mei-yu season was observed: one in 1954 with 50 days and the other in 1980 with 43 days. However, for 1991, if the pre-Mei-yu period of 18–27 May (see below) is included, the total 1991 Mei-yu season can be as long as 56 days, thus making it the longest Mei-yu season for the last 40 yr.

Second, the heavy precipitation covered a large area. Figure 1 shows the spatial distribution of 1991 total precipitation (averaged over 18 May–13 July when heavy precipitation occurred) and precipitation anomaly (vs the 1981–90 means). Most of the areas over YHRV had precipitation more than 700 mm. The 500-mm contours concentrated along an elongated area of northeast–southwest orientation. Although this rain belt orientation remains relatively unchanged in 1991 (vs the climatological means), the intensity was much stronger. For example, the precipitation increased by 50% over the whole YHRV, and some areas had amounts more than three times the long-term averages. On the other hand, the data showed a below-normal precipitation in the regions north and south of YHRV. This pattern of floods in the middle and drought in the north and south occurs frequently throughout historical times in China (Liang et al. 1995).

Third, persistent heavy precipitation occurred throughout June and July. This characteristic can be seen in Fig. 2, in which the daily precipitation for three latitudinal zones in 1991 was plotted against the 1981–90 mean daily values. Here, the observed precipitation is calculated using daily data from the World Meteorological Organization surface networks with 171 stations in China. There are clear differences in the observed precipitation evolution among these three zones. The most distinct characteristic is the existence of clear breaks between heavy precipitation events in YHRV (30°–34°N), while the southern zone showed relatively continuous precipitation (except for two short periods during the middle and end of May) and the northern zone had much smaller precipitation amounts. For YHRV, except for two short breaks, heavy precipitation occurred from mid-May to mid-June. It resumed again at the end of June and continued to mid-July. Note that heavy precipitation over YHRV at the end of July and

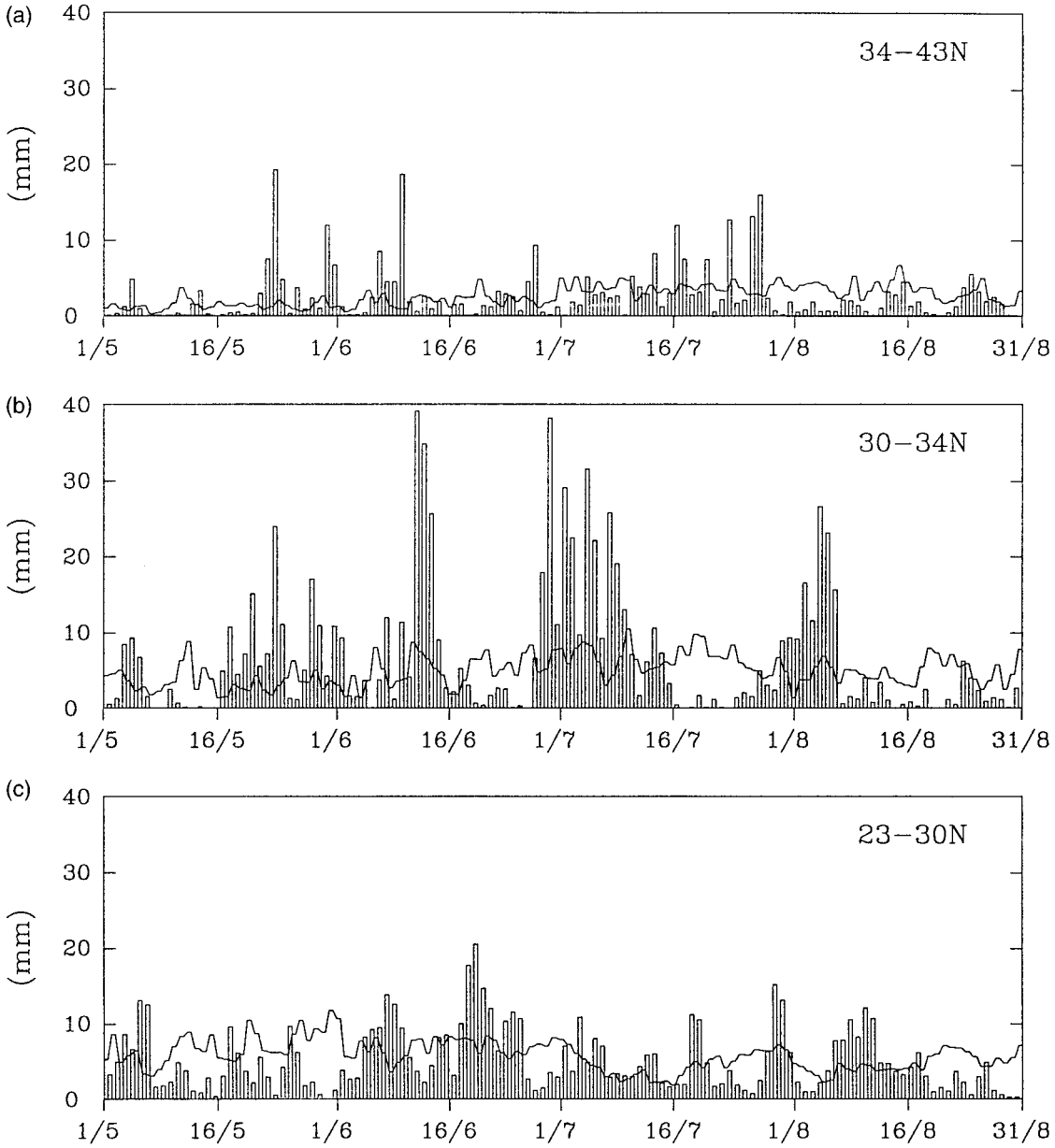

FIG. 2. Observed daily precipitation (mm) averaged over 105°–122°E for 1991 (bars) and 1981–90 climatological mean (lines). The data are from the same source as in Fig. 1 and with 71, 36, and 64 stations, respectively, in the 34°–43°N (northern), 30°–34°N (central), and 23°–30°N (southern) latitudinal zones.

early August was associated with typhoons, which are the seasonal events for this region. Except for a few short periods in 1991, precipitation deficiency was generally found north and south of YHRV.

As mentioned earlier, the precipitation anomaly over YHRV is always related to the large-scale anomalous circulation. Here, we concentrate on the three circulation components of the Mei-yu system: the upper-tropospheric westerly jet described by the 200-hPa zonal wind; the WPSH represented by the 5880 geopotential meter (gpm) of the 500-hPa geopotential height; and the southwest monsoon flow illustrated by the 850-hPa wind. Figure 3 shows the June monthly mean statistics of these fields averaged over 1981–90 as well as their 1991 anomalies. It is known that the westerly jet has a profound effect on precipitation over eastern China (Liang and Wang 1998). It is quite clear that the jet became much enhanced over Japan and Korea in 1991, which induced a strong ''indirect'' circulation on the plane across the jet stream and thus favored heavy precipitation in the south (i.e., left side of the entrance) of the jet. The precipitation over YHRV is closely linked to the WPSH with persistently

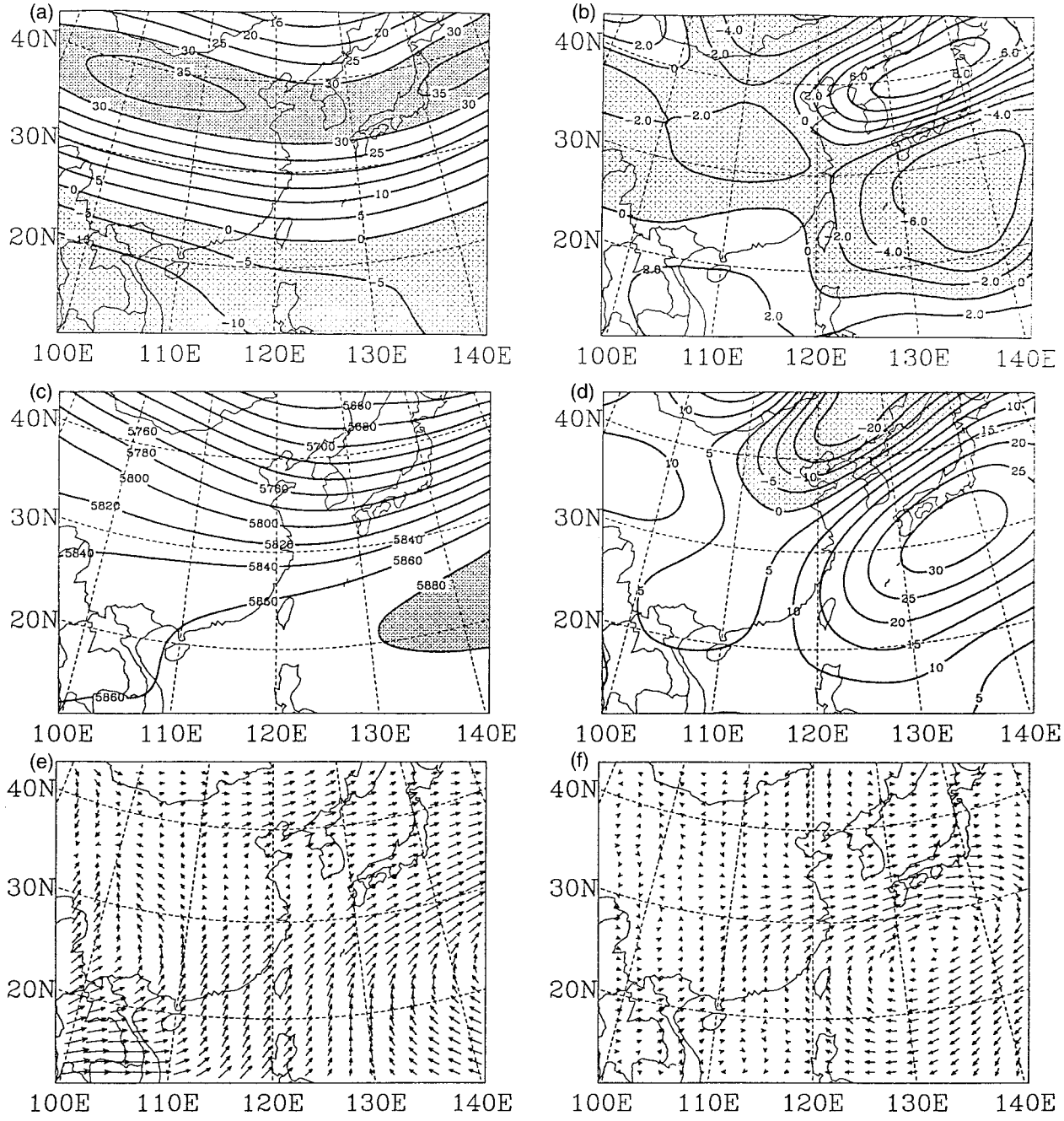

FIG. 3. (a) 1981–90 Jun monthly mean 200-hPa zonal wind (m s^{-1}) and (b) the 1991 deviation from the 10-yr mean. Contours greater than 30 m s^{-1} (less than 0 m s^{-1}) are densely (lightly) shaded. (c) 1981–90 Jun monthly mean 500-hPa geopotential height and (d) the 1991 deviation from the 10-yr mean (gpm). Contours greater than 5880 gpm (less than 0 gpm) are densely (lightly) shaded. (e) 1981–90 Jun monthly mean 850-hPa vector wind and (f) the 1991 deviation form the 10-yr mean.

strong WPSH between 20° and 25°N over East Asia during pre-Mei-yu and Mei-yu periods (see Tao and Chen 1987). The 1991 WPSH had two characteristics: stronger in its intensity than the 10-yr climatological mean and thus heavy precipitation over YHRV; and stably situated between 19° and 24°N producing an earlier and longer rainy season (Ding 1993). The southwest monsoon flow at 850 hPa was also very strong in 1991, especially from the middle and lower reaches of the Yangtze River to south of Japan. The enhanced monsoon flow brought in more warm and moist air from the south to generate a heavy Mei-yu.

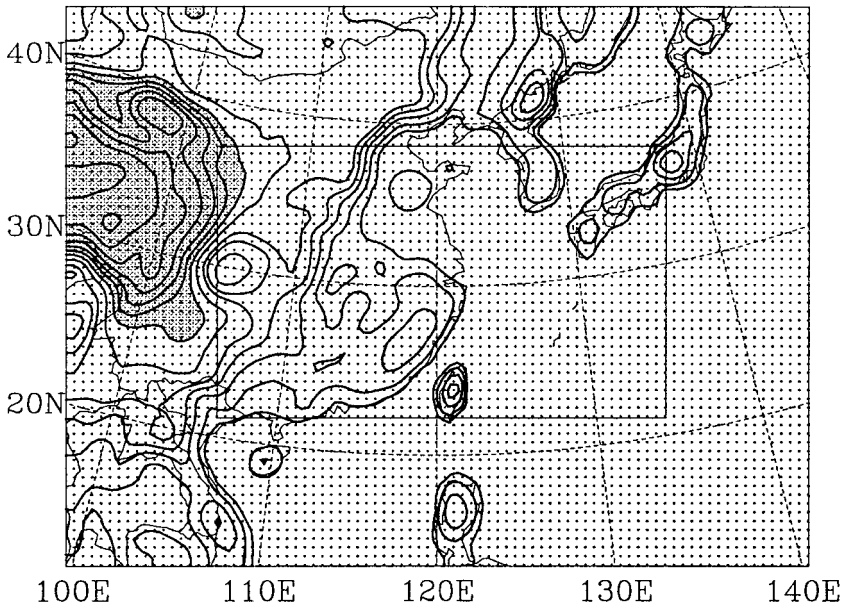

FIG. 4. Model domain and topography (m) for the regional climate simulations. The model grid spacing is 60 km with 85 and 65 grid points, respectively, in the west–east and south–north directions. The area between the outer and inner frames denotes the 18-gridpoint buffer zone used in the experiments (see section 3).

3. Model description

The SUNYA RCM (Dudek et al. 1996) is used to conduct simulations of the 1991 summer monsoon over East Asia. The dynamic structure of the model is the same as that of the Pennsylvania State University–National Center for Atmospheric Research Mesoscale Model version 5 (MM5; Grell et al. 1994), which uses terrain-following sigma (σ) vertical coordinate, $\sigma = (P - P_T)/(P_S - P_T)$, where P, P_T, and P_S denote pressure at each model level, model top pressure, and the prognostic surface pressure, respectively. The model uses 23 levels in the vertical with model top at 10 hPa. The simulation domain (shown in Fig. 4) centered over the lower reaches of the Yangtze River (30°N and 120°E) covers an area of 5040 km $\times$ 3840 km including East Asia and adjacent western Pacific Ocean. The eastern slope of the Tibetan Plateau, which has a peak elevation of over 5000 m, is located at the western edge of the domain. The horizontal gridpoint spacing is 60 km, and at this resolution, prominent features of the topography in western China, the coastline, and some isolated mountains in Japan, Korea, Northeast and southeast China, Taiwan, and north of the Philippines are captured. Note that there are at least two issues associated with the western boundary of the Tibetan Plateau. As discussed in Gong and Wang (2000), a lack of measurements introduces large uncertainties in the driving field used for input to the regional model. In addition, the incorporation of appropriate topography also poses a challenge to the modeling community. Nevertheless, in the present study, we have somewhat arbitrarily specified the western boundary to be along 90°–100°E.

The model physics include: Anthes–Kuo cumulus convective scheme (Anthes et al. 1987), a ''force-restore'' slab model developed by Blackadar (Zhang and Anthes 1982) to calculate the surface temperature, a revised version of Blackadar's high-resolution boundary layer model to calculate the vertical mixing of horizontal wind, potential temperature, water vapor mixing ratio, cloud water, and ice (not used in this study). Note that we have not implemented the vegetation–soil scheme in the model, which, as shown later, induced some errors in the simulation; and that the surface sensible and latent heat fluxes calculated by the Blackadar's scheme are based on the MM5 inherent treatment of soil moisture, which may be inconsistent with the very wet soil in the YHRV region during spring and summer of 1991 (see Ding 1993). An explicit treatment of cloud water, rainwater, snow, and ice (Dudhia 1989) was used to treat precipitation physics. For radiation parameterization, we used the longwave scheme of Wang et al. (1991) while the shortwave scheme is based on Thompson and Pollard (1995). More discussion of the radiation parameterization was given in Liang et al. (1995) while its use in RCM for comparison with measurements at the southern Great Plains was included in Dudek et al. (1996). A diagnostic cloud–radiation parameterization developed by Liang and Wang (1995) was used to simulate the cloud fractions, which together with the prescribed cloud optical properties for different cloud types (convective cloud, anvil cirrus, stratiform cloud, and inver-

sion stratus) were used for radiative heating/cooling calculations. Note that in this paper we excluded the inversion stratus in the cloud–radiation parameterization because it induces errors, as discussed in Gong and Wang (2000).

To run the regional model, meteorological initial conditions and lateral boundary forcing of winds, temperature, water vapor mixing ratio, and surface pressure are needed. In the present study, these data were interpolated from the European Centre for Medium–Range Weather Forecasts (ECMWF)–Tropical Ocean Global Atmosphere (TOGA) objective analysis, which is available every 12 h with a resolution of 2.5° × 2.5° in the horizontal and 15 pressure levels up to 10 hPa. Vertical interpolation from these pressures to the model level is linear in pressure for wind and relative humidity, and linear in the logarithm of pressure for temperature. For model grids over the ocean, Navy sea surface temperature (SST) was used and updated twice daily by interpolating SST data (63 × 63 grids for the Northern Hemisphere) onto the RCM grids and integration time steps.

We used the relaxation procedure of Davies (1976) as the coupling scheme, which specifies how the large-scale lateral boundary forcings provided by the objective analysis are being used by the regional climate model. The most important aspect of this procedure is determined by two factors: the distribution function of the nudging coefficient and the width of the buffer zone. Sensitivity experiments, documented in Gong and Wang (2000), were conducted to examine the effects of different choices on the simulations. As concluded by Gong and Wang (2000), the combination of a linear distribution function and an 18-gridpoint buffer zone (Fig. 4), which we used here, provides the best simulation results.

For the comparison between model simulations and observations, the model value at the grid point closest to a surface station was used as the model value at that station. We used the following measures, which are similar to those used by Giorgi et al. (1993), in the diagnostics:

1) Model error, Er, for daily parameter a averaged over a region with N stations

$$\mathrm{Er} = \frac{1}{N}\sum_{i=1}^{N}(a_i^m - a_i^o), \tag{1}$$

where superscripts m and o refer to model and observation, respectively. Here, Er measures how the model average climatology deviates from observed value.

2) Spatial correlation coefficient, Cs, for monthly mean parameter b between simulation and observation over a region with N stations

$$\mathrm{Cs} = \frac{\sum_{i=1}^{N}(b_i^m - \overline{b}^m)(b_i^o - \overline{b}^o)}{\left[\sum_{i=1}^{N}(b_i^m - \overline{b}^m)\sum_{i=1}^{N}(b_i^o - \overline{b}^o)\right]^{1/2}}, \tag{2}$$

where the overbar denotes spatial averages. Here, Cs measures the agreement between observed and simulated spatial patterns.

3) Temporal correlation coefficient, Ct, for spatially averaged parameter c during a period of N days

$$\mathrm{Ct} = \frac{\sum_{i=1}^{N}(c_i^m - \overline{c}^m)(c_i^o - \overline{c}^o)}{\left[\sum_{i=1}^{N}(c_i^m - \overline{c}^m)\sum_{i=1}^{N}(c_i^o - \overline{c}^o)\right]^{1/2}}, \tag{3}$$

where the overbar denotes temporal averages. Here, Ct measures the agreement between simulated and observed trends of the parameters.

4) Spatial standard deviation, Ss

$$\mathrm{Ss} = \left[\frac{\sum_{i=1}^{N}(a_i - \overline{a})^2}{N-1}\right]^{1/2}, \tag{4}$$

which is a measure of spatial variability of the variable a.

4. Simulation results

The regional model was integrated continuously from 1 May to 31 July, covering the summer monsoon period in 1991. In the present study, the analyses focus on two aspects of the simulations: the evolution of the Mei-yu front, in particular over YHRV, and its association with circulation components of the Mei-yu system; and the consistency among these circulation components.

a. Precipitation and temperature

The model-to-observation comparison of the daily precipitation for three latitudinal zones is shown in Fig. 5. For YHRV, there were three heavy precipitation periods: the pre-Mei-yu (Early Yellow Mei-yu or Zao Huang Mei) period from 18 May to 26 May; the first period of Mei-yu from 2 June to 19 June; and the second period of Mei-yu from 30 June to 13 July. The simulation clearly catches these heavy precipitation events and break periods, although the simulated precipitation intensities are smaller, especially during the peaks at mid-June and throughout the first half of July. The difference can be a factor of two to three smaller, thus reflecting the inadequacy of the regional model to simulate the magnitude of precipitation fluctuations. It is interesting to note that better agreement in both magnitude and phase is simulated in the southern zone.

The observed and simulated May–July mean precip-

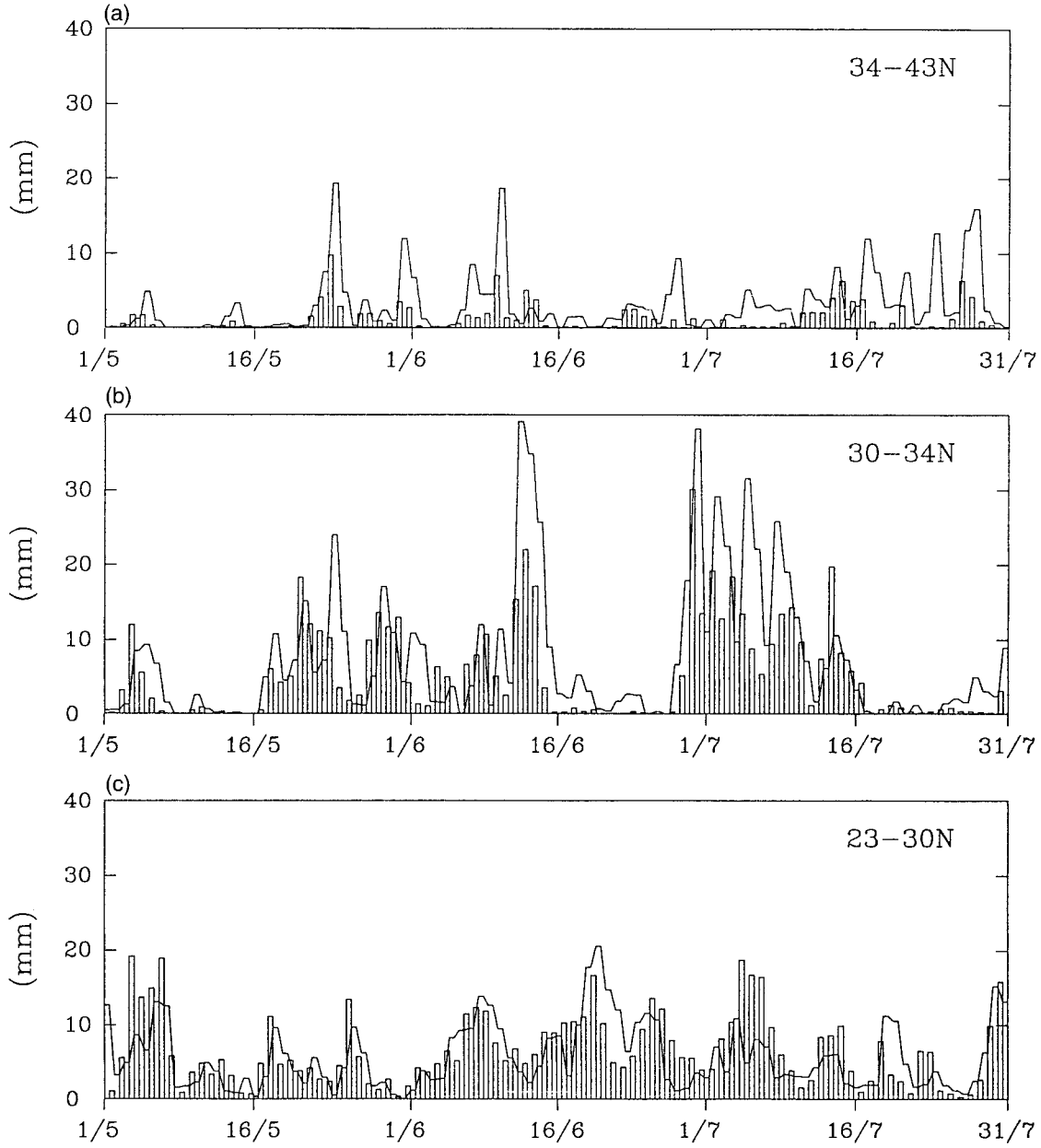

FIG. 5. 1991 observed (lines) and model-simulated (bars) daily precipitation for the indicated three latitudinal zones averaged between 105° and 122°E. The observations are from the same source as in Fig. 1.

TABLE 2. May–Jul mean statistics of observed and simulated precipitation (mm day^{-1}) and surface air temperature (°C) averaged over the area (23°–43°N; 105°–122°E). Here Cs and Ct are the spatial and temporal correlation coefficients, respectively.

Parameter	Observation	Simulation	Cs	Ct
Precipitation	5.01	4.18	0.54	0.70
Temperature	23.29	22.83	0.96	0.94

itation and surface air temperature for the region (23°–43°N; 105°–122°E) are compared in Table 2. The model simulates reasonably well the regional mean precipitation and temperature in the region, with model error (Er) of -0.83 mm day^{-1} and -0.46°C, respectively. For surface air temperature, both spatial and temporal correlation is quite high, with coefficients at 0.96 and 0.94, respectively. The model also captures reasonably well the trend of precipitation (0.70) over the region, which is consistent with results shown in Fig. 5. The correlation coefficient of the spatial pattern for precipitation is, however, relatively small. To further investigate this

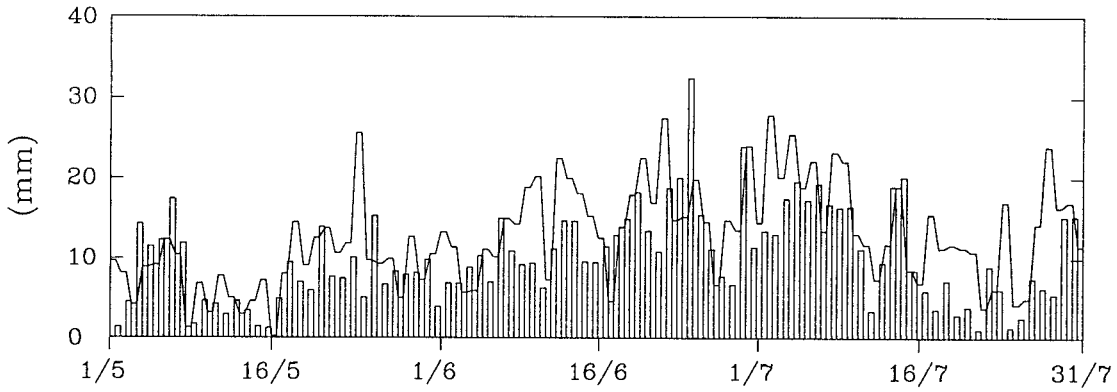

FIG. 6. The daily variation of spatial standard deviation of precipitation calculated over the region (105°–122°E, 23°–43°N). The solid line and bars are for observation and simulation, respectively.

deficiency, we analyzed the spatial standard deviation (Ss) of precipitation, calculated over the region, for both the observation and simulation (Fig. 6). Clearly, the model reproduces reasonably well the trend of observed spatial pattern of precipitation. However, the spatial variability seems to be generally underestimated by the model.

The smaller model-simulated Mei-yu precipitation over YHRV can be attributed to two model deficiencies. First, the southward shift (vs the observations) of the simulated Mei-yu front is consistent with a simulated colder atmosphere, which results in a southward shift of the location where the cold air from the north meets the warm air from the south. Second, the model lower atmosphere is also found to be drier, especially over the central part of the simulation domain. The moisture bias can be attributed to the coupling scheme, which will also be discussed in more detail in Gong and Wang (1999), and to a lack of vegetation-soil scheme in the land surface process model (see Dickinson et al. 1989).

b. Monthly mean circulation statistics

As discussed before, there are several circulation components of the Mei-yu system that are strongly associated with the Mei-yu front. Because of a lack of available observational data, we use the ECMWF–TOGA analysis as a reference. Note that these comparisons are more meaningful for statistics averaged over certain longitude zones, simply because the objective analysis is generated from low-resolution models (see Gong and Wang 2000). In addition, the comparisons can yield useful information when we examine the consistency of the Mei-yu system (rather than the individual components) between model simulations and objective analysis.

The evolution of 200-hPa zonal wind averaged over 110°–120°E is shown in Fig. 7. The analyzed westerlies for the first half of May were the strongest with peak values over 40 m s^{-1} covering wide latitudinal zones north of 28°N. In mid-May the westerlies were significantly weakened. Toward the end of May, strong westerlies reappeared at locations farther north while the easterlies developed in the regions south of 27°N. This is the result of eastward movement of the South Asian high, which induces an anticyclonic circulation (i.e., westerlies in the north and easterlies in the south) in the upper troposphere. The anticyclonic circulation provides a proper divergence condition aloft for the low-level convergence along the Mei-yu front over YHRV. This pattern occurred again in the middle of June and early July, although the magnitude for the latter period was smaller. Starting in mid-July, the westerlies became weaker and moved farther north with an accompanying northward expansion of the easterlies, indicating a northward movement of the anticyclone. In comparison, the model simulates very well the patterns of intensification and break of the westerlies, and their northward movements, although the magnitudes of the jet streams especially at 35°–40°N are weaker. In addition, there is a tendency for the simulated westerlies and easterlies to shift farther south. This feature is also consistent with the model ''cold'' bias (see Table 2) and the southward dislocation of the simulated Mei-yu front discussed above.

The 500-hPa geopotential height averaged over 120°–130°E (the oceanic region) is shown in Fig. 8. The observed WPSH, represented by the contour of 5880 gpm (see Ding 1994) had the tendency to strengthen as time progressed into summer, although breaks occurred. These features are closely associated with precipitation over YHRV. For example, a major break occurred during the second half of June when there was no precipitation over YHRV (see Fig. 5). On the other hand, starting at the end of June and for most of the first half of July, the WPSH reached 27°–30°N when heavy precipitation occurred over YHRV. The model simulates very well the magnitude and phase of the 500-hPa height, including the location of WPSH, which can be partially attributed to the use of observed SST. Similar comparison is made over the land areas 110°–120°E (not shown). The simulated WPSH also agrees well with the

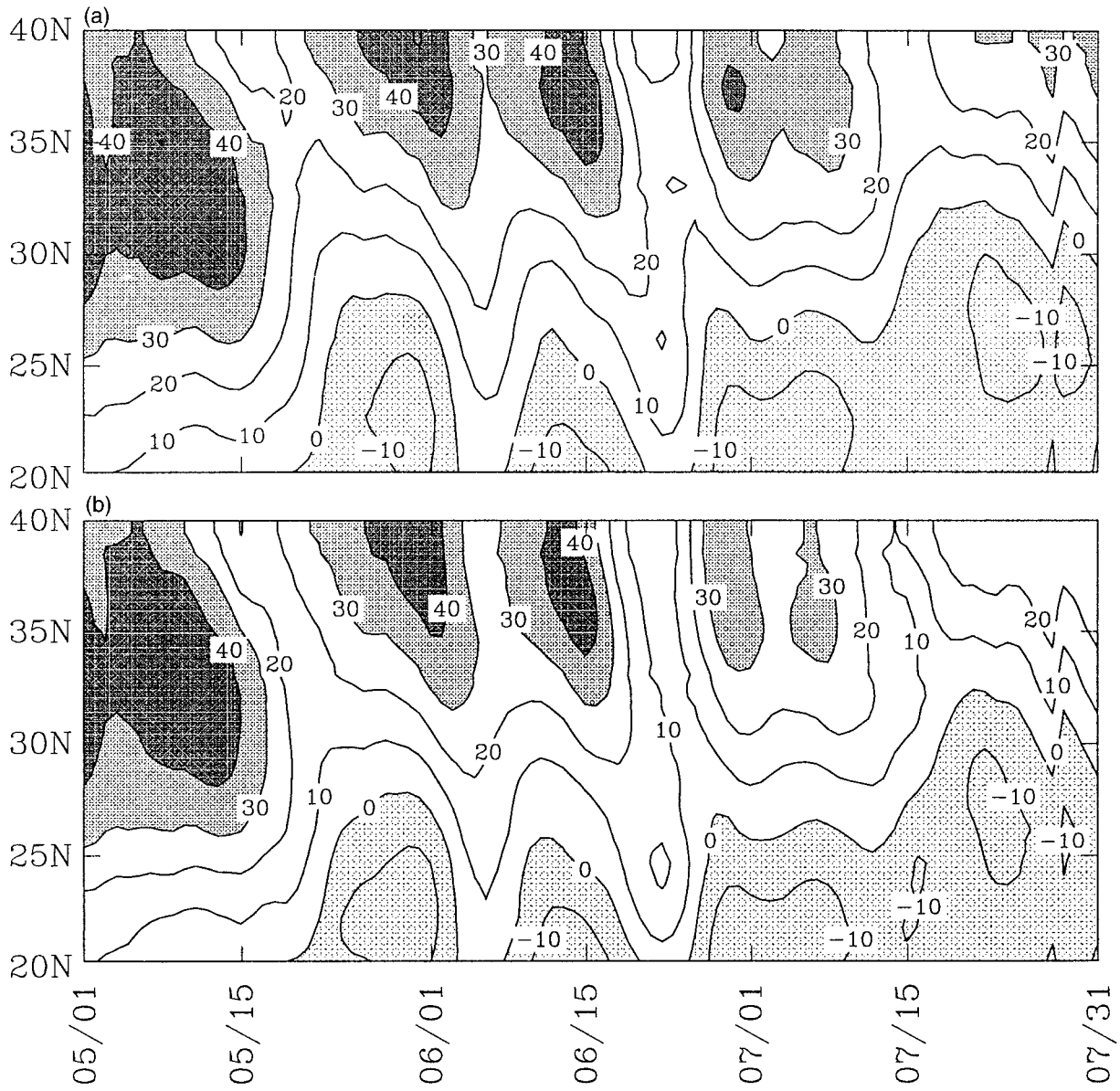

FIG. 7. (a) 1991 ECMWF–TOGA and (b) model-simulated time-latitudinal variations of 200-hPa zonal wind (m s^{-1}) averaged between 110° and 120°E. Shaded contours, from light to dark, are less than 0 m s^{-1} and greater than 30 and 40 m s^{-1}, respectively.

objective analysis, although its location is somewhat displaced farther south of the analyzed subtropical high location, especially after the middle of July. This southward displacement is again related to the simulated ''colder'' (vs the observation) atmosphere, in which the subtropical high is not sufficiently strong to move into the cold region in the north (beyond 26°N). The results further illustrate the importance of the land surface processes in affecting (through the surface temperature) the evolution of large-scale circulation.

During the pre-Mei-yu and Mei-yu periods of 1991, the objective analysis, shown in Fig. 9, indicates intensified 850-hPa meridional wind in the regions located south of the Yangtze River Valley (30°N) during 17–26 May, 6–13 June, and 27 June–15 July. This is consistent with previous observations that heavy precipitation is frequently accompanied by low-level jet (Tao and Chen 1987; Ding 1994). The jet stream transports abundant moisture and unstable warm air behind the Mei-yu front located in the north and produces heavy precipitation over YHRV. The model simulations indicate similar characteristics, although the intensities are slightly larger and the lengths are also longer especially for the last period. Note that the locations of these Maxima are also farther south, and therefore the shearline of the Mei-yu front shifted southward in the simulation, a feature consistent with the model ''cold'' bias. Similar features are also found in the 850-hPa zonal wind (not shown).

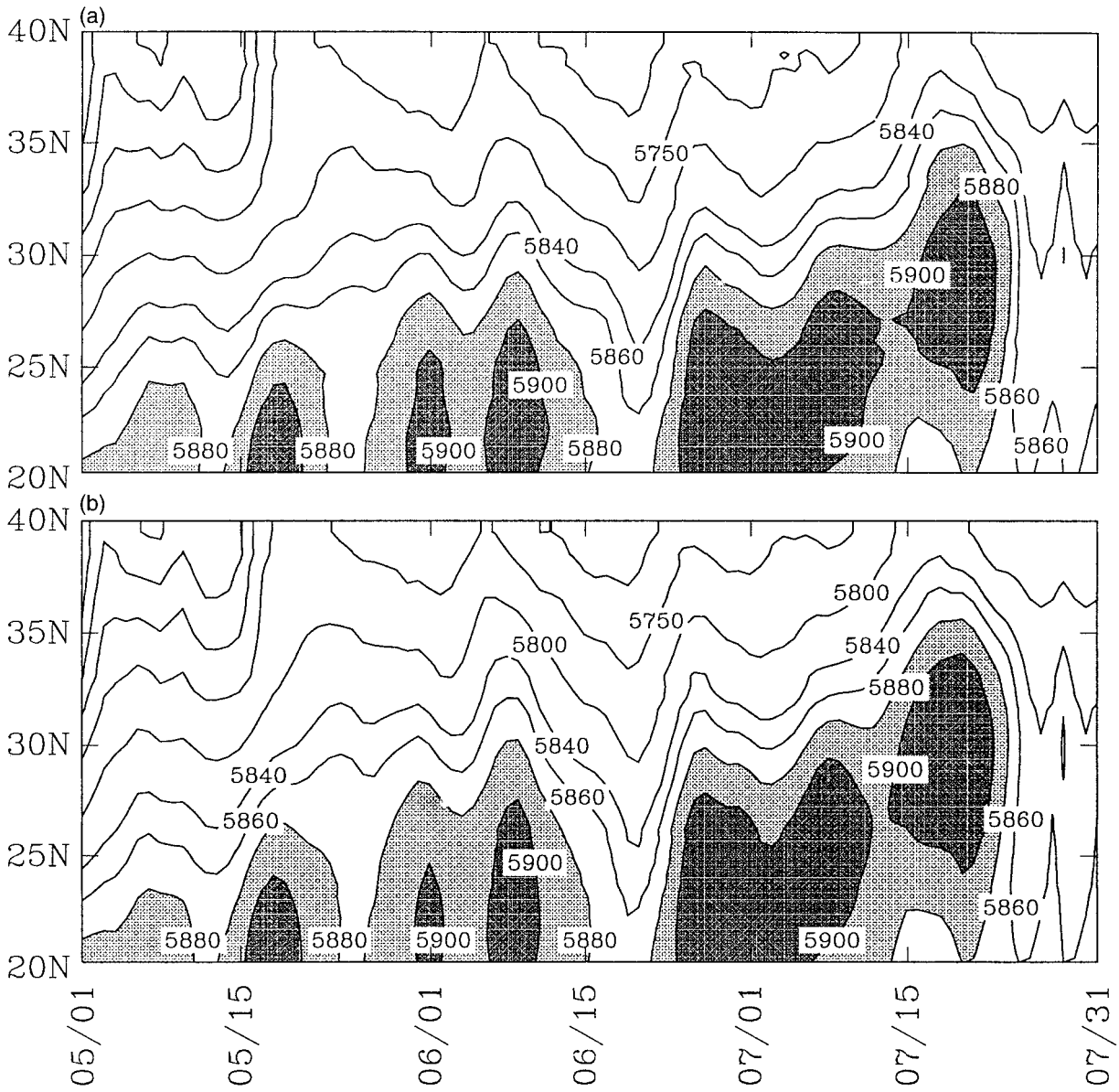

FIG. 8. (a) 1991 ECMWF–TOGA and (b) model-simulated time-latitudinal variations of 500-hPa geopotential height (gpm) averaged between 120° and 130°E. Contours greater than 5880 (5900) gpm are lightly (darkly) shaded.

Although the model has bias in simulating the magnitude and phases of the individual components (e.g., 200-hPa zonal wind) of the Mei-yu system, these components are however consistent among themselves. To illustrate the point, we use the evolution of the WPSH averaged over 120°–130°E (Fig. 8) to examine its consistency with other circulation components. During the Mei-yu season in 1991, the WPSH has substantial seasonal changes in its location and strength. For example, during the pre-Mei-yu period in mid-May, the WPSH in the analysis retreated to south of 20°N on 13 May, and then suddenly jumped to 27°N on 17 May. In the same period, the westerly jet at 200 hPa (Fig. 7) also experienced a dramatic jump, from its mean latitude of 33°N (15 May) to 40°N (29 May). It is interesting to note that the jump of the WPSH happened when the westerly jet disappeared in the north. Meanwhile, the 850-hPa meridional wind over 20°–40°N (Fig. 9) also changed direction from north to south around 15 May. In response to the changes (i.e., strengthening and southward shifting) of the WPSH, the 850-hPa zonal wind (not shown) was suddenly enhanced south of the YHRV on 16 May. These concurrent features indicate that there exists a close relationship among these circulation components. In similar fashion, the Mei-yu front also moves (from South China) northward to YHRV, in response to

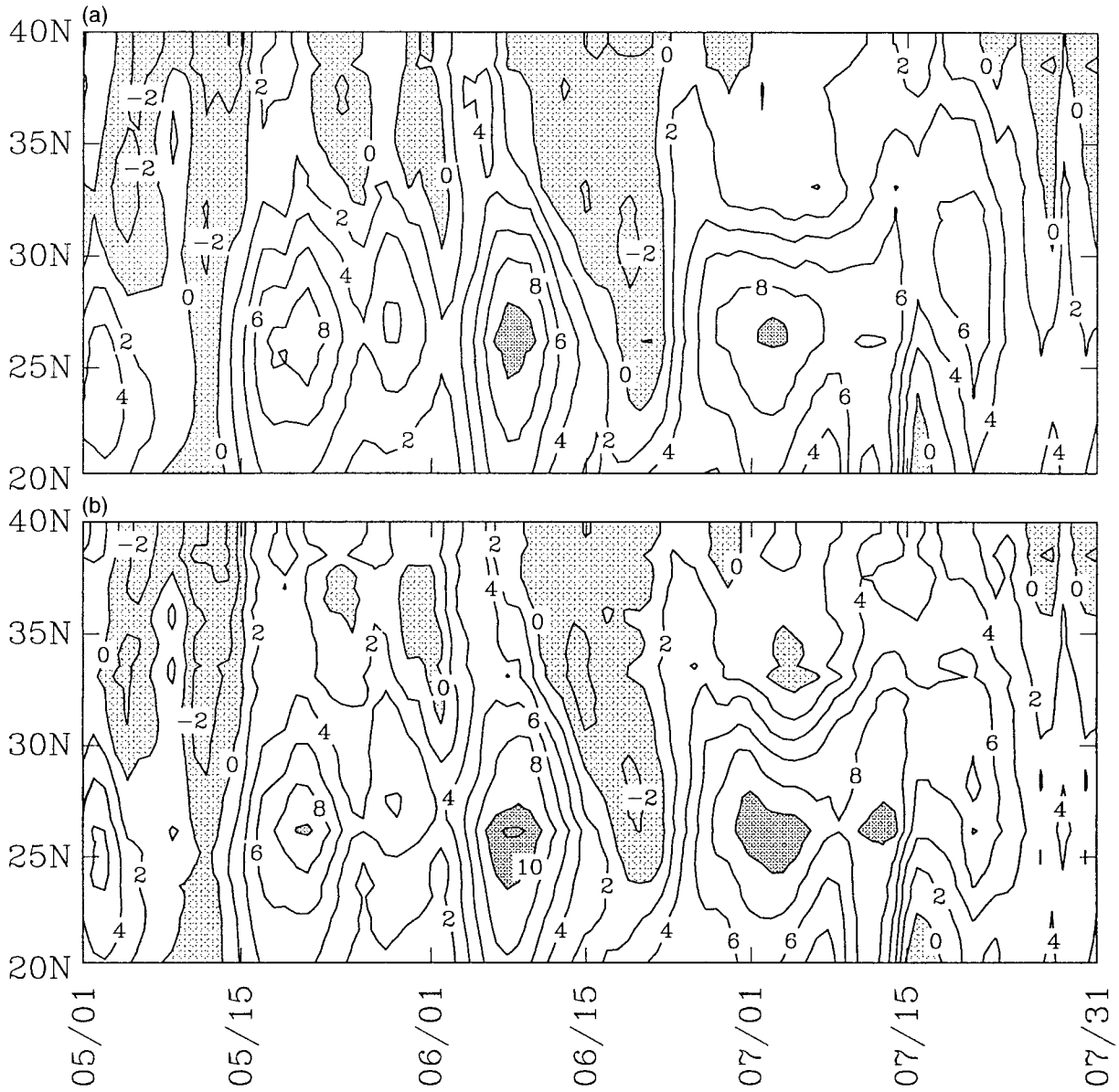

FIG. 9. Same as in Fig. 7 but for 850-hPa meridional wind (m s^{-1}). Contours less than 0 m s^{-1} (greater than 10 m s^{-1}) are lightly (darkly) shaded.

seasonal changes of the circulation components. All these internal consistencies can also be seen in the model simulations.

In addition, the simulated components of the Mei-yu system also show consistent short-term fluctuations, as found in the observational analyses for 1991 (Lu and Ding 1997) and for other years (Ding 1994). For example, the WPSH retreated from its extreme northern latitude of 29°N on 9 June to south of 20°N on 15 June (Fig. 8). Correspondingly, the 200-hPa westerly jet is intensified and shifted southward at midlatitudes before the middle of June (Fig. 7). It was also evident that the retreat of the WPSH is related to the expansion of cold air with the low-level zonal wind suddenly decelerated after 14 June. Meanwhile the meridional wind changes from southerly to northerly, indicating the southward shift of Mei-yu front due to the intrusion of cold air from the north; this aspect will be further discussed in section 4c. Again, the model simulations show similar characteristics.

These consistencies in the relationship among circulation components identified in both the model and objective analysis is encouraging and it further demonstrates the reliability of the dynamical and physical based model. Further improvement on model deficiency, such as the model ''cold'' bias, may lead to a better

simulation of the precipitation over YHRV especially after 15 July when the simulated subtropical high over the land area (110°–120°E) did not advance farther northward, as found in the objective analysis.

c. Short-term variation of the Mei-yu system

Given the consistency of the circulation components on a monthly basis, we further examine the simulated evolution of the Mei-yu system on a shorter timescale. Note that, in addition to the circulation components discussed above, there are other factors, for example, the ITCZ in the South China Sea and blocking highs at high latitudes, which have significant effects on the Mei-yu system. These factors, however, cannot be considered here because of the model spatial domain used. Therefore, we analyze only the association and relationship among several relevant field—200-hPa westerly jets at midlatitude, 500-hPa WPSH, vertically integrated moisture flux, and the Mei-yu front, which are simulated within the domain.

The heavy precipitation over YHRV is a result of interaction between the Mei-yu front and tropospheric moisture divergence/convergence (Tao and Chen 1987). In the present analysis, we used heavy precipitation ($>$7.5 mm day^{-1}) to describe the location of the Mei-yu front and strong composite wind (greater than 35 m s^{-1}) for the upper-tropospheric westerly jet. Because of its close relevance to the heavy precipitation events (Yamazaki and Chen 1993), we used the vertically integrated moisture flux to reveal the potential weakness of the cumulus parameterization. In the analysis, we used 5-day mean as the averaged period to analyze the evolution of the Mei-yu front. The period is chosen so that the daily fluctuation can be smoothed out.

Comparisons of the observed and simulated evolution of the Mei-yu system from June to mid-July are shown in Figs. 10 and 11, respectively. In each figure, the 5-day mean values of 200-hPa westerly jet, the WPSH, vertically integrated moisture flux, and precipitation distribution are depicted. Note that the measured precipitation is used in the figures. Before discussing the association and relationship among these components, we first examine the evolution of the rain belt. In 1991, YHRV experienced two severe precipitation periods: 11–15 June and 1–10 July, during which the daily mean precipitation amount exceeded 30 mm day^{-1}. In general, the simulated precipitation pattern (orientation and sometimes magnitude and location) agrees reasonably well with the observations throughout the above two periods. For example, the simulation reproduces well the southwest–northeast orientation for the first 10 days of July. The model also catches the precipitation Maxima in the south during the Mei-yu onset phase and over the northeast during the Mei-yu withdrawal phase.

Clearly, there are also major deficiencies in the simulated precipitation. The model simulated rain belts generally stay farther south of the observations, thus yielding an underestimation of precipitation over the middle reaches of the Yangtze River. While the observed precipitation has Maxima over YHRV, the simulated centers are located at the southwest end of the rain belt during 11–15 June and 11–15 July. In addition, the model generally simulates smaller precipitation over the entire domain, especially over YHRV. One exception is for the period 11–15 July when the Mei-yu season ended and the typhoon season started in South China. For 1991, close relation is found between the end of the Mei-yu season and typhoon activity in coastal areas of South China (Ding 1993). However, during this period, heavy precipitation still persists along the Mei-yu front and subtropical high does not jump northward in the simulation, caused by the colder temperature resulting from a lack of land surface process model (see Gong and Wang 2000).

On the other hand, the model simulates better the association between precipitation patterns and circulation components as well as the relationship among the individual components. For example, for the period of 1–5 June when the Mei-yu season began, there existed an upper-tropospheric westerly jet centered around 40°N and confined within 120°–130°E. In the south, subtropical high located at south of 28°N blocked the moisture transport from the south, and resulted in weak precipitation over the Yangtze River valley. In the next pentad, the core of the westerly jet moved eastward, indicating that cold air was weakened in the north; at the same time, the subtropical high also weakened, and moved to the coastline of South China. The eastward movement of WPSH allowed southwest moist air to reach YHRV and resulted in moderate precipitation. Furthermore, because of the weakening of cold air in northern China, monsoon flow brought moisture farther northward and induced a relatively strong precipitation near Beijing and its surrounding area. For 11–15 June, the WPSH was slightly intensified in the south, while the upper-tropospheric westerly jet was greatly enhanced in the north. Thus, the cold air along the westerly jet and warm air pushed by the WPSH converged over YHRV. In the meantime, abundant moisture, mainly from Southeast Asia and partly from the South China Sea and the western Pacific Ocean, converged over YHRV. As a result, the first heavy precipitation event occurred. During the next 5 days, cold air was further intensified accompanying the southeast shift of the westerly jet, while the weakened WPSH retreated to the oceanic area east of 125°E. Under this circumstance, the maximum of vertically integrated moisture flux also moved southward to the South China Sea. Moderate precipitation occurred in South China. For 21–25 June, the cold air in the north strengthened due to the deepening of the trough in East Asia, and the upper-tropospheric westerly jet reached the area in South China. At this time, frontal precipitation occurred over the ocean. The second severe precipitation event 25 June–15 July showed similar characteristics, except that much longer period of interac-

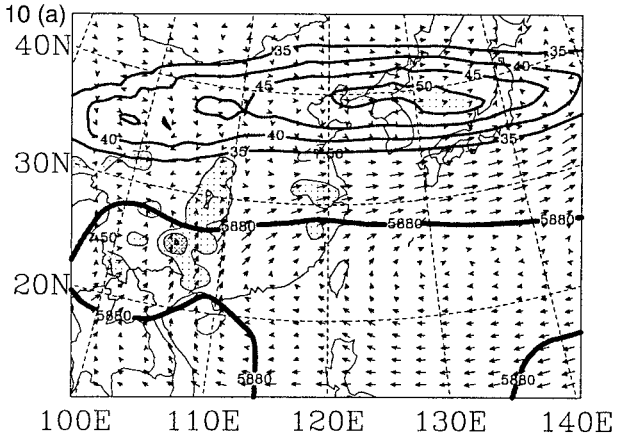

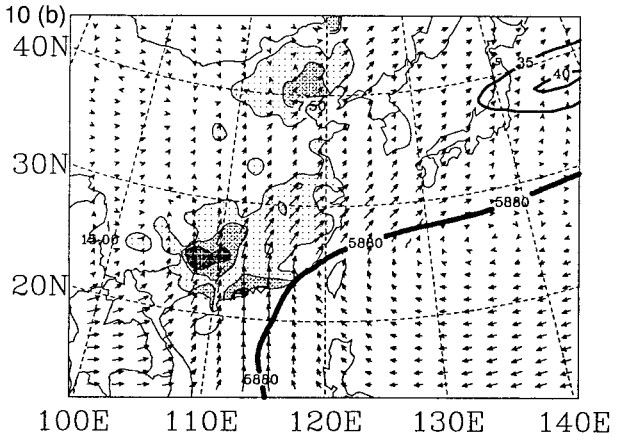

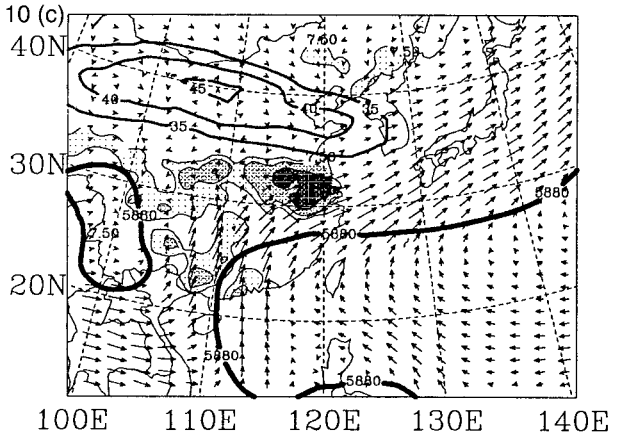

FIG. 10. Five-day mean of ECMWF–TOGA 200-hPa westerly jet (composite wind speed above 35 m s^{-1}), 500-hPa subtropical high (line of 5880 gpm, thick), vectors of vertically integrated moisture fluxes, and observed heavy precipitation (lightly shaded contours for 7.5 mm day^{-1}, densely shaded for 15 mm day^{-1}, and dark shaded for 30 mm day^{-1}) during the 1991 Mei-yu season, for (a) 1–5 Jun, (b) 6–10 Jun, (c) 11–15 Jun, (d) 16–20 Jun, (e) 21–25 Jun, (f) 26–30 Jun, (g) 1–5 Jul, (h) 6–10 Jul, and (i) 11–15 Jul. Contours of observed precipitation were only drawn over eastern China.

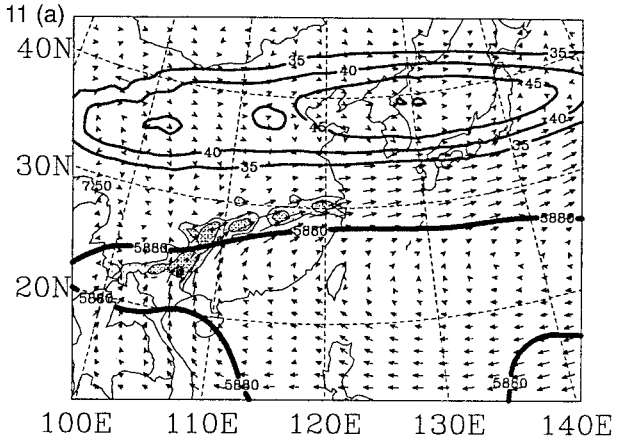

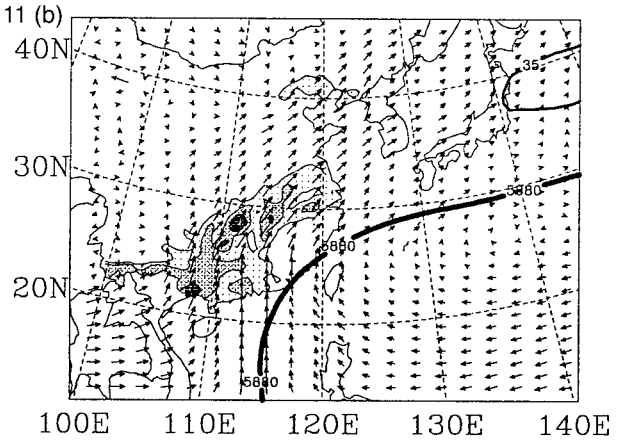

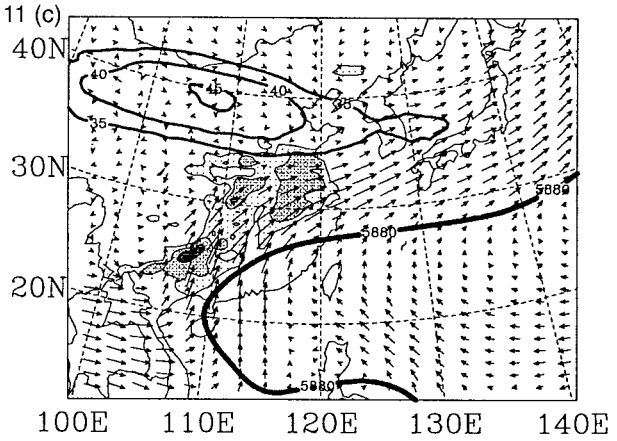

FIG. 11. Same as in Fig. 11 but for model simulation.

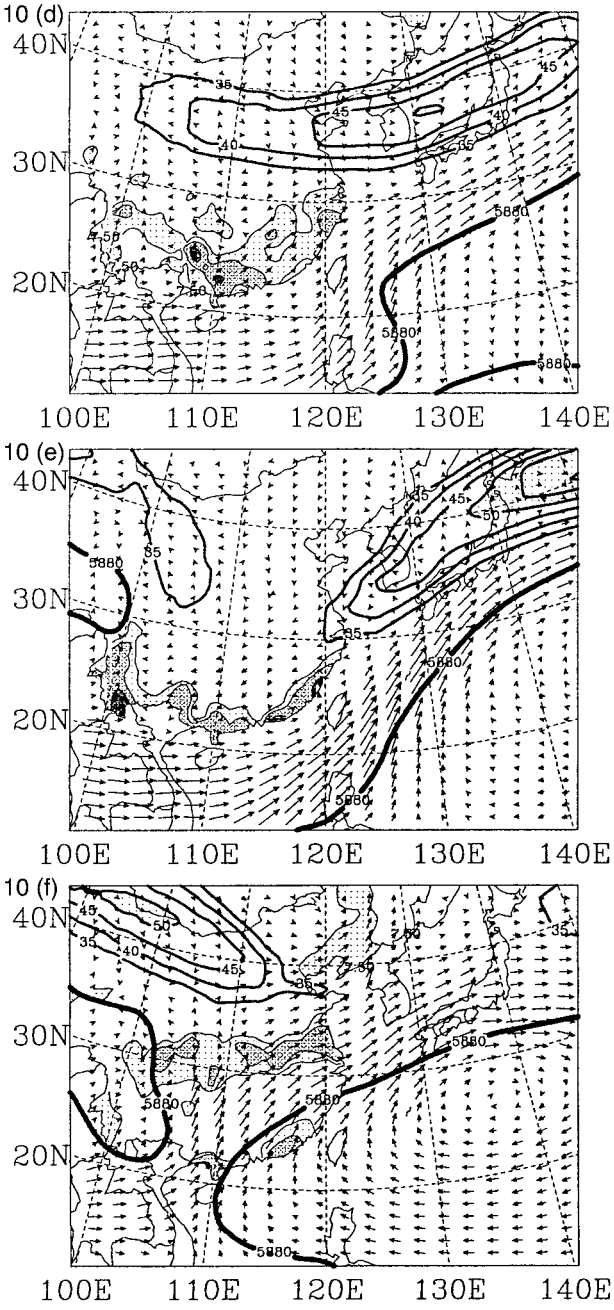

FIG. 10. (*Continued*)

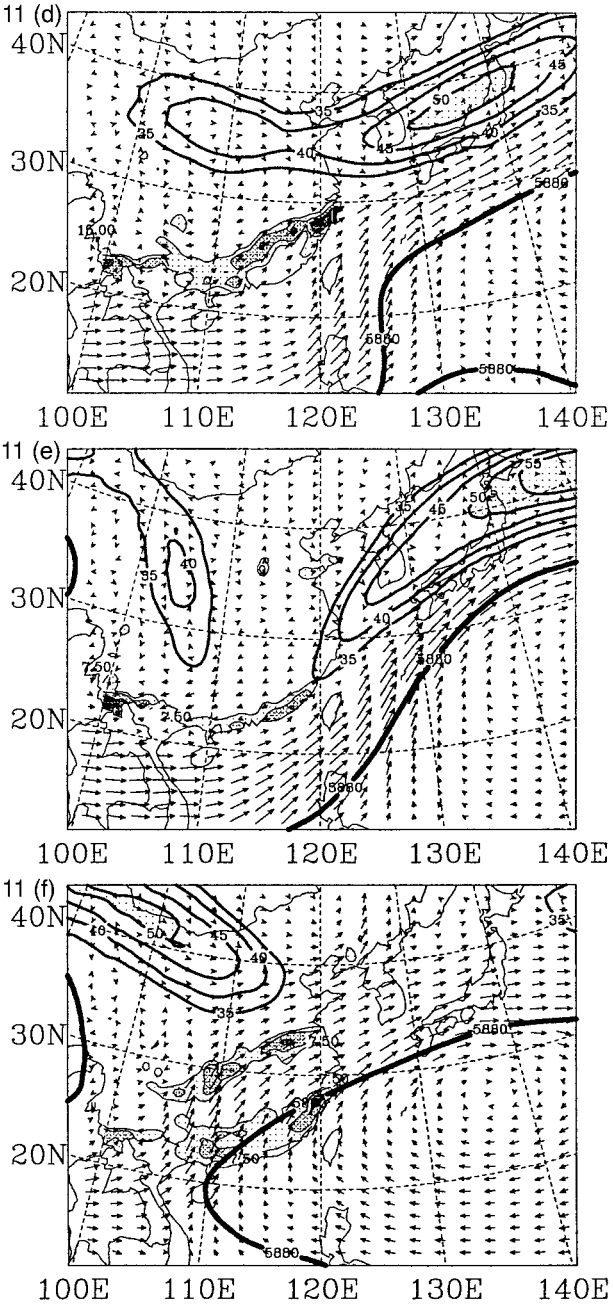

FIG. 11. (*Continued*)

tions between cold air from the north and warm air from the south occurred over YHRV, which resulted in extremely heavy precipitation. In addition, several points are also worth commenting on here.

First, analyses of both model simulations and objective analysis indicate the close association between heavy precipitation, and the strength and location of strong moisture fluxes; this is consistent with the findings of Yamazaki and Chen (1993), who studied the structure of the Baiu front south of Japan. In addition, the strong moisture fluxes, usually located a few hundred kilometers northwest of the edge of subtropical high, is usually associated with a low-level jet (or strong wind) around 850 hPa. Although many mechanisms (see Chen 1982; Chou et al. 1990; Chen and Li 1995) were proposed to explain this feature, clearly the dynamical effect of the subtropical high plays an essential role.

Second, the location of the Mei-yu front during severe precipitation events is always located between the westerly jet and subtropical high, irrespective of

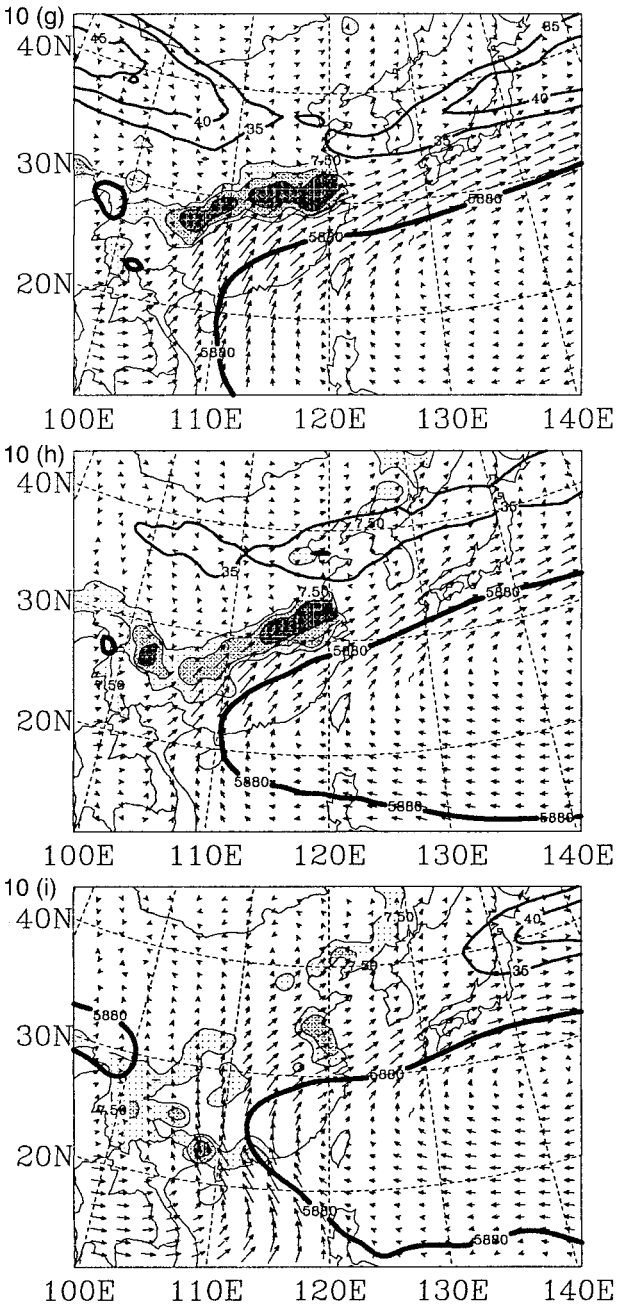

FIG. 10. (*Continued*)

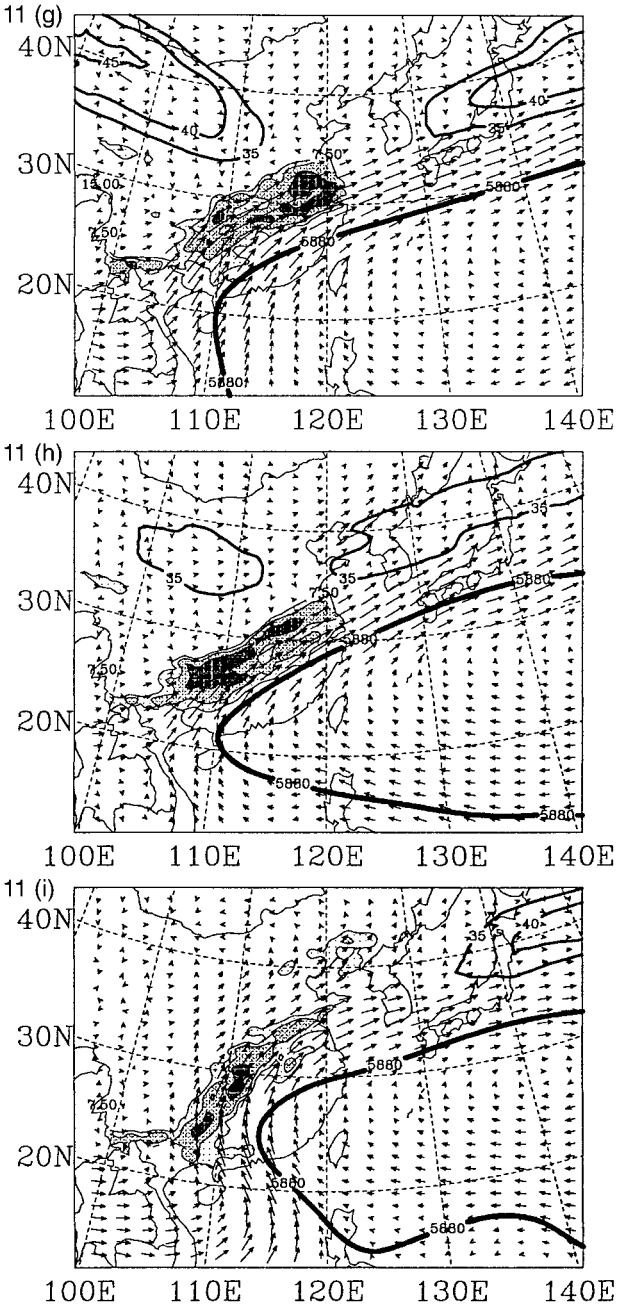

FIG. 11. (*Continued*)

whether the front is over YHRV or other places. This feature was also found in the Baiu front of Japan (Yamazaki and Chen 1993). Generally speaking, for the simulated period the westerly jet has two strong centers: one over northwest China and the other over the Pacific Ocean near Japan. It is the former center that has the greatest influence over YHRV. For example, several heavy precipitation events occur when this jet streak situates itself or passes by the areas north of YHRV. The model simulates fairly well the relationship of jet-WPSH-Mei-yu throughout the integration, although the simulated locations of these components shift slightly to the south.

Third, moisture for heavy precipitation events over YHRV usually comes mainly from the South China Sea and to a lesser extent from the Bay of Bengal in June, and from the Bay of Bengal, the South China Sea, and western Pacific in July (see Ding 1994). The moisture source for 1991 was somewhat different. Except for 1–5 June when moderate moisture fluxes are

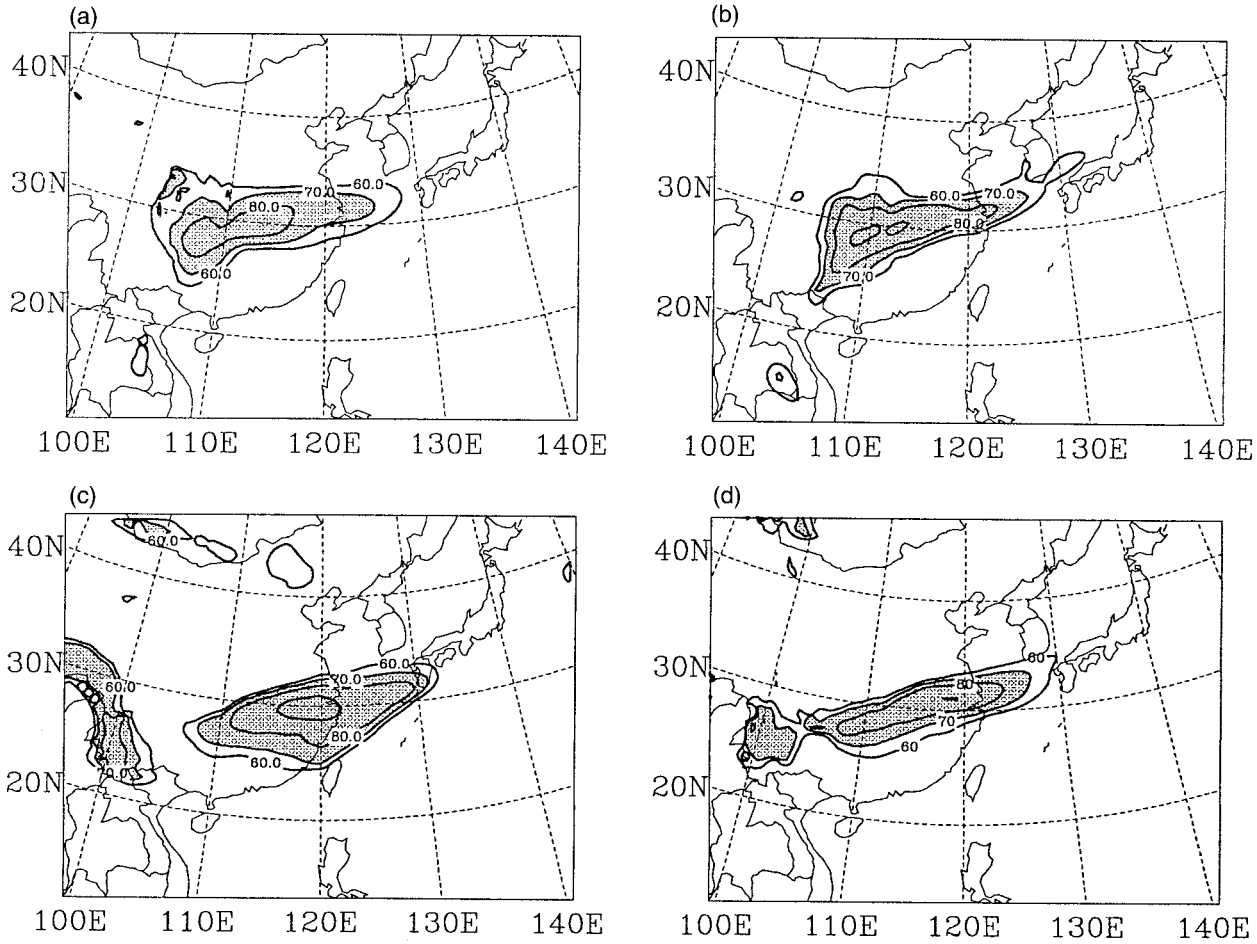

FIG. 12. (a) and (b) Correlation coefficient (%) between the mean precipitation over the area (30°–34°N, 105°–122°E) and 850-hPa water vapor mixing ratio from (left panels) ECMWF–TOGA and (right panels) model simulation. (c) and (d) Same as in upper panels except for 850-hPa water vapor flux. Same observed precipitation as in Fig. 2 is used in the calculation of correlation with ECMWF–TOGA objective analysis. The coefficients were calculated at each model grid point for the period of 18 May and 13 Jul. Contours greater than 70 are lightly shaded. Five-day running mean was applied to precipitation, water vapor mixing ratio, and magnitude of water vapor flux before calculating the correlation coefficient.

found over the South China Sea and the western Pacific, moisture for the rest of June was transported by the west and southwest flows from the Bay of Bengal with small contribution from the western Pacific. During the first half of July, moisture flux from the Bay of Bengal dominated the period of 1–5 July and 11–15 July, while, for the rest of July, moisture sources over the western Pacific Ocean, Bay of Bengal, and the South China Sea were of equal importance. Ding (1993) suggested that there exists a relationship between severe Mei-yu events and the enhanced convective activities over the Bay of Bengal because of their effects in accumulating atmospheric water vapor.

d. Correlation between precipitation over YHRV and Mei-yu components

As discussed above, it is encouraging to find that the model is capable of simulating not only the evolution of the individual components of the Mei-yu system, but their interactions as well. To further illustrate this point, we calculate the correlation between mean precipitation averaged over YHRV and 850-hPa water vapor mixing ratio as well as the water vapor flux over the domain. The correlation is calculated using 5-day running mean values of these quantities for the period 18 May–14 July. Two sets of correlations were evaluated, one based on observed precipitation and ECMWF–TOGA analysis, and the other on simulated precipitation and atmospheric fields. Because ECMWF–TOGA analysis is also based on observations, we may use it as the basis to evaluate model performance. Note that the objective analysis has coarser resolution than RCM.

The correlation between the precipitation over YHRV and the 850-hPa water vapor mixing ratio is shown in Fig. 12. The result indicates high correlation exists for both sets of comparisons along 30°N. This is expected because precipitation is positively associated with water

vapor amount. However, the correlation for RCM is slightly higher, especially for the upper reaches of the Yangtze River west of 110°E, thus indicating that the simulated precipitation is more sensitive to the water vapor amount. The correlation between precipitation and magnitude of 850-hPa water vapor flux are also shown in Fig. 12. Again, high correlation exists for both the model and analysis. A correlation coefficient exceeding 0.9 is found over the Yangtze River valley (120°E and 30°N) for 850-hPa wind in the ECMWF–TOGA analysis. This correlation indicates the effect of location and strength of low-level moisture flux (south of the Mei-yu front) on Mei-yu precipitation, which was pointed out in the observational study by Tao and Chen (1987). The RCM also adequately reproduces the above correlation pattern (e.g., the orientation), thus suggesting that the model indeed simulates the association between Mei-yu precipitation and low-level moisture flux. On the other hand, we also notice slightly smaller correlation coefficients in the model simulations, which reflect an underestimate of the effect of dynamical convergence, a major weakness associated with the cumulus parameterization.

5. Conclusions and discussion

The Mei-yu over East Asia is the result of multiscale interactions. Regional climate models, which include details of the regional characteristics with time-dependent lateral boundary forcing provided by objective analysis, are a useful tool for studying these interactions. In the present study, we used the State University of New York at Albany (SUNYA) Regional Climate Model to simulate the 1991 severe precipitation event over the Yangtze–Huai River valley (YHRV). The objective is to evaluate the model's capability in simulating the evolution of the Mei-yu system in which the scale interactions play a major role. Note that the simulations are based on the best model configuration concluded from the sensitivity studies documented in the companion paper (Gong and Wang 2000).

It is shown that the model simulates well not only the regional mean precipitation and temperature, the time evolution of the individual components of the Mei-yu system (200-hPa jet, 500-hPa geopotential height, 850-hPa winds, and tropospheric moisture flux), but also the relationship among these components. Analyses of 5-day mean circulation statistics and their associations with the evolution of Mei-yu indicate that 200-hPa westerly jet at midlatitudes, 500-hPa subtropical high, and vertically integrated moisture flux are strongly associated with severe precipitation events. It is also found that different phases (onset, mature, and withdraw) of the Mei-yu front are closely related to changes in large-scale circulation. However, the model has problems in simulating some of the circulation components over land areas after the end of the Mei-yu season. As a result, the simulated rain belt still stayed south of YHRV after 14 July. This inadequacy can be attributed to the cold bias resulting from weaknesses in the model's parameterization schemes for land surface processes.

It should be noted here that, in addition to the lower boundary effects, the regional model is subject to a variety of inherent uncertainties, in particular the lateral boundary forcing used to drive the simulation. A critical issue is the treatment of one-way interaction, which mainly concerns the large-scale to regional-scale without considering the feedback. This is important since the regional domain is an open system in the sense that the moisture and energy fluxes across the lateral boundary have strong influence on the domain simulations. To address this aspect, we have conducted many sensitivity experiments to examine the extent to which the model biases are associated with the treatment of lateral boundary conditions. These results are summarized in Gong and Wang (2000).

To properly model the climate over East Asia requires several improvements over the lower boundary. First, the present simulation domain is located at 100°E, which slices through the Tibetan Plateau. In so doing, the effects of both dynamical and thermal forcing are not properly considered (D.-Z. Ye 1998, personal communication). Second, and perhaps more critical to the simulation of YHRV precipitation and surface air temperature, is the lack of a vegetation–soil scheme in the regional model to account for the boundary forcing of both energy and moisture flux. Third, in the view of regional climate prediction, an interactive ocean model for the oceanic region is also necessary, although it may pose a great challenge. These aspects, especially the first two, are currently being addressed in our ongoing research at SUNYA.

Acknowledgments. The research was supported by Biological and Environmental Research, Office of Science, U.S. Department of Energy.

REFERENCES

Anthes, R. A., E.-Y. Hsie, and Y.-H. Kuo, 1987: Description of the Penn State/NCAR Mesoscale Model version 4 (MM4). NCAR Tech. Note, NCAR/TN-282+STR, National Center for Atmospheric Research, Boulder, CO, 66 pp. [Available from NCAR, P.O. Box 3000, Boulder, CO 80307.]

Chen, C.-S., W.-S. Chen, and Z.-S. Deng, 1991: A study of a mountain-generated precipitation system in northern Taiwan during TAMEX IOP 8. *Mon. Wea. Rev.,* **119,** 2574–2606.

Chen, G. T.-J., and C.-C. Yu, 1988: Study of low-level jet and extremely heavy rainfall over northern Taiwan in the Mei-yu season. *Mon. Wea. Rev.,* **116,** 884–891.

Chen, Q., 1982: The instability of the gravity–inertia wave and its relation to low-level jet and heavy precipitation. *J. Meteor. Soc. Japan,* **60,** 1041–1057.

Chen, Y.-L., and J. Li, 1995: Large-scale conditions favorable for the development of heavy rainfall during TAMEX IOP 3. *Mon. Wea. Rev.,* **123,** 2978–3002.

Chou, L. C., C.-P. Chang, and R. T. Williams, 1990: A numerical simulation of the Mei-yu front and the associated low level jet. *Mon. Wea. Rev.,* **118,** 1408–1428.

Davies, H. C., 1976: A lateral boundary formulation for multilevel prediction models. *Quart. J. Roy. Meteor. Soc.*, **102,** 405–418.

Dickinson, R. E., R. M. Errico, F. Giorgi, and G. T. Bates, 1989: A regional climate model for the western U.S. *Climatic Change*, **15,** 383–422.

Ding, Y.-H., 1993: *Research on the 1991 Persistent, Severe Flood over Yangtze–Huai River Valley* (in Chinese). Chinese Meteorological Press, 255 pp.

——, 1994: *Monsoons over China.* Kluwer Academic Publishers, 419 pp.

Domros, M., and G. Peng, 1988: *The Climate of China.* Springer-Verlag, 360 pp.

Dudek, M.-P., X.-Z. Liang, and W.-C. Wang, 1996: A regional climate model study of the scale dependence of cloud–radiation interactions. *J. Climate*, **9,** 1221–1234.

Dudhia, J., 1989: Numerical study of convection observed during the winter monsoon experiment using a mesoscale two-dimensional model. *J. Atmos. Sci.*, **46,** 3077–3107.

Giorgi, F., G. T. Bates, and S. Nieman, 1993: The multiyear surface climatology of a regional atmospheric model over the western United States. *J. Climate*, **6,** 75–95.

Gong, W., and W.-C. Wang, 2000: A regional model simulation of 1991 severe precipitation event over Yantze–Huai River Valley. Part II: Model bias. *J. Climate*, **13,** 93–108.

Grell, A. G., J. Dudhia, and D. R. Stauffer, 1994: A description of the fifth-generation Penn State/NCAR mesoscale model (MM5). NCAR Tech. Note NCAR/TN-398+STR, National Center for Atmospheric Research, Boulder, CO, 122 pp. [Available from NCAR, P.O. Box 3000, Boulder, CO 80307.]

Lau, K.-H., A.-Y. Wang, Y.-H. Kuo, S.-J. Chen, and J. Dudhia, 1998: The evolution of the East Asia summer monsoon in June 1994: Numerical simulations. *J. Meteor. Soc. Japan*, **76,** 749–764.

Lau, K.-M., and M.-T. Li, 1984: The monsoon of East Asia and its global association—A survey. *Bull. Amer. Meteor. Soc.*, **65,** 116–125.

——, and S. Yang, 1996: Seasonal variation, abrupt transition, and intraseasonal variability associated with the Asian summer monsoon in the GLA GCM. *J. Climate*, **9,** 965–985.

Leung, L. R., S. J. Ghan, Z.-C. Zhao, Y. Luo, W.-C. Wang, and H.-L. Wei, 1999: Intercomparison of regional climate model for simulation of the 1991 Summer Monsoon in East Asia: Special issue on ''New Development and Applications in Regional Climate Models.'' *J. Geophys. Res.*, **104,** 6425–6454.

Liang, X.-Z., and W.-C. Wang, 1995: A GCM study of the climatic effect of 1979–1992 ozone trend. *Atmospheric Ozone as a Climate Gas*, W.-C. Wang and I. S. A. Isaksen, Eds., NATO ASI Series, Vol. 32, Springer-Verlag, 259–288.

——, and ——, 1998: Associations between China monsoon rainfall and tropospheric jets. *Quart. J. Roy. Meteor. Soc.*, **124,** 2597–2623.

——, ——, and M. P. Dudek, 1995: Interannual variability of regional climate and its change due to the greenhouse effect. *Global Planet. Change*, **10,** 217–238.

Liu, Y.-Q., R. Avissar, and F. Giorgi, 1996: Simulation with the regional climate model RegCM2 of extremely anomalous precipitation during the 1991 East Asian flood: An evaluation study. *J. Geophys. Rev.*, **101,** 26 199–26 216.

Lu, E., and Y.-H. Ding, 1997: Low frequency oscillation in East Asia during the 1991 excessively heavy rain over the Changjiang–Huaihe River basin. *Acta Meteor. Sin.*, **11,** 12–22.

Samel, A. N., S. Wang, and W.-C. Wang, 1995: A comparison between observed and GCM-simulated summer monsoon characteristics over China. *J. Climate*, **8,** 1690–1696.

Sperber, K. R., S. Hammed, G. L. Potter, and J. S. Boyle, 1994: Simulation of the northern summer monsoon in the ECMWF model: Sensitivity to horizontal resolution. *Mon. Wea. Rev.*, **122,** 2461–2481.

Tao, S.-Y., and L.-X. Chen, 1987: A review of recent research on the East Asian summer monsoon in China. *Monsoon Meteorology*, C.-P. Chang and T. N. Krishnamurti, Eds., Oxford University Press, 60–92.

Thompson, S. L., and D. Pollard, 1995: A global climate model (GENESIS) with a land surface transfer scheme (LSX). Part I: Present-day climate. *J. Climate*, **8,** 732–761.

Wang, H.-J., 1997: On the modeling study of monsoon. *Acta Meteor. Sin.*, **11,** 119–128.

Wang, W.-C., G.-Y. Shi, and J. T. Kiehl, 1991: Incorporation of the thermal radiative effect of CH_4, N_2O, $CFCl_3$, and CF_2Cl_2 into the NCAR community climate model. *J. Geophys. Res.*, **96,** 9097–9103.

Yamazaki, N., and T.-C. Chen, 1993: Analysis of the East Asian monsoon during early summer of 1979: Structure of the Baiu front and its relationship to large-scale fields. *J. Meteor. Soc. Japan*, **71,** 339–355.

Ye, D.-Z., 1988: The thermal structure and the convective activity over Qinghai–Tibetan Plateau in summer and their interactions with large-scale circulation (in Chinese). *Sci. Atmos. Sin.*, 1–12.

Zhang, D.-L., and R. A. Anthes, 1982: A high-resolution model of the planetary boundary layer: Sensitivity tests and comparisons with SESAME-79 data. *J. Appl. Meteor.*, **21,** 1594–1609.